

Oscillator Basics and Low-Noise Techniques for Microwave Oscillators and VCOs

Ulrich L. Rohde* (ulr@synergymwave.com)
Chairman, Synergy Microwave Corporation

GaAs 2000 – Paris, France
2-6 October 2000

Abstract

Microwave oscillator design is based on the principle of generating a negative resistance to compensate for the losses of the resonator. Several circuit combinations, including one- and two-port oscillators, are possible. In this discussion, we will first evaluate the conditions of oscillation for the Colpitts and Clapp-Gouriet oscillator. We will then evaluate a 19-GHz SiGe-based oscillator by assuming values, backed up by available S parameters and dc I - V curves, that we assigned to the nonlinear BFP520 model. So far it has been difficult to obtain complete documentation on modeling for the SiGe transistors, but our approximation appears to be justified. Next, we will evaluate a ceramic-resonator-based oscillator and show its performance. Going up to higher frequencies, we will introduce a 47-GHz lumped-resonator oscillator and a VCO at the same frequency that uses GaAsFETs as varactors. In all cases, we will give a thorough treatment of the circuits and their performance.

Introduction

This presentation will give an overview of both bipolar and GaAsFET-based oscillators, including ceramic-resonator oscillators (CROs). Its purpose is to show not only the linear/nonlinear mathematics, but also how the actual design should be considered, as well as commentary on the results. Many of the predictions can only be obtained by using appropriate software; for this purpose, we have used a harmonic-balance simulator by Ansoft. We also will show some practical circuits, both from the circuit design as well as the actual chip design. In the assumptions we have taken, we have avoided shortcuts so that the approach remains general in nature. It further needs to be pointed out that throughout this discussion, we will assume that each oscillator is followed by an isolation stage that can handle the input power, has at least 10 dB of amplification, and provides isolation of more than 30 dB. An FET amplifier is ideal because it will load the oscillator very little.

Basic Oscillator Conditions

An oscillator is an electronic circuit that overcomes the losses of a resonator by applying energy at the resonator frequency into the resonator. This and the initial switch-on transient will start oscillation, and the oscillator's amplitude will be limited and stabilize based on the nonlinearities of the active device(s). What really happens is that the transistor will change its dc transconductance at startup condition into a new dc transconductance and a transconductance

* Department of Electrical Engineering, Universities of Oradea, Bradford, and George Washington.

value for the fundamental frequency and its harmonics. The total sum of these transconductances needs to be the same as the starting value at a given dc point. This is the mechanism that

stabilizes the oscillation and creates harmonic content, including a dc level shift that reduces the actual loop gain to exactly 1.

The required necessary (negative) resistance to compensate for the losses and enable oscillation is calculated by

$$R_n = -\frac{\text{Re}(S_{21})}{50 \times \omega^2 \times C_1 \times C_2} \quad (1)$$

Figure 1 shows the voltage divider of the Colpitts oscillator

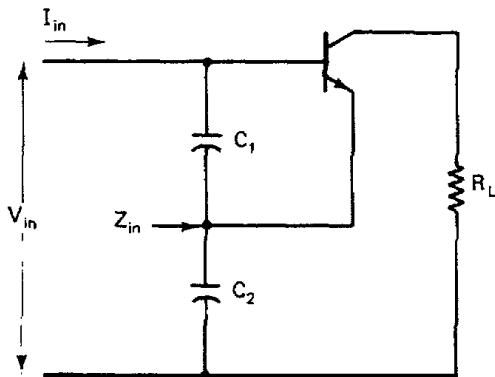


Figure 1-- Input of a Colpitts oscillator; the capacitive divider generates a negative input resistance which will start oscillation if an inductor is added.

The value of S_{21} can be obtained from the datasheet and the resulting R_n should be negative and sufficiently large to compensate the losses. On the other hand, there is a limit to how large the capacitance can be made. As the capacitance increases, the magnitude of R_n gets smaller and will no longer be large enough to compensate the losses. To demonstrate this, we have plotted in Figure 2 the real and imaginary values of the input impedance Z_{11} of Port 1 of the circuit shown in Figure 4.

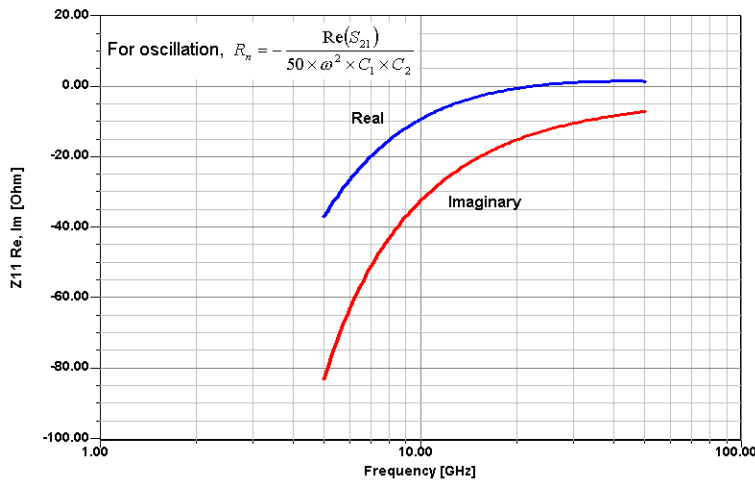
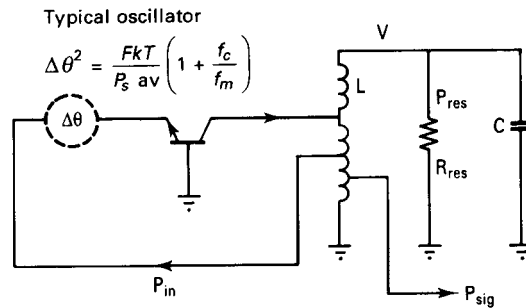


Figure 2--Real and imaginary values for Z_{11} . Z_{11} must be slightly larger than the loss resistance in the circuit for oscillation to start. The resulting dc shift in the transistor will then provide the amplitude stabilization.

Figure 3 shows a feedback oscillator illustrating the principles involved and showing the key components considered in the phase-noise calculation and its contribution. While this is a grounded-base oscillator, it can be transformed into any other configuration.



For $f_m < \frac{f_o}{2Q_{load}}$

$$L_{c}(f_m) = \frac{1}{2} \frac{1}{\omega_m^2} \left(\frac{\omega_o}{2Q_{load}} \right)^2 \frac{FkT}{P_s \text{ av}} \left(1 + \frac{f_c}{f_m} \right)$$

$$Q_{load} = \frac{\omega_o W_6}{P_{diss, total}} = \frac{\omega_o W_6}{P_{in} + P_{res} + P_{sig}}$$

$$= \frac{\text{Reactive power}}{\text{Total dissipated power}}$$

Maximum energy in C or L : $W_6 = \frac{1}{2} C V^2$

$$L_{c}(\omega_m) = \frac{1}{8} \frac{FkT}{P_s \text{ av}} \frac{\omega_o^2}{\omega_m^2} \left(\frac{P_n}{\omega_o W_6} + \frac{1}{Q_{unl}} + \frac{P_{sig}}{\omega_o W_6} \right)^2 \left(1 + \frac{\omega_c}{\omega_m} \right)$$

Phase Perturbation
Resonator Q
Flicker Effect

Input power over Reactive Power
Signal power over Reactive Power

Figure 3--Diagram for a feedback oscillator illustrating the principles involved and showing the key components considered in the phase-noise calculation and its contribution.

The Colpitts Oscillator

For very high frequency applications, the Colpitts oscillator and a variation of this, correctly called the Clapp-Gouriet, are the circuits of choice. The following section deals with the standard Colpitts oscillator, which was chosen for our first example.

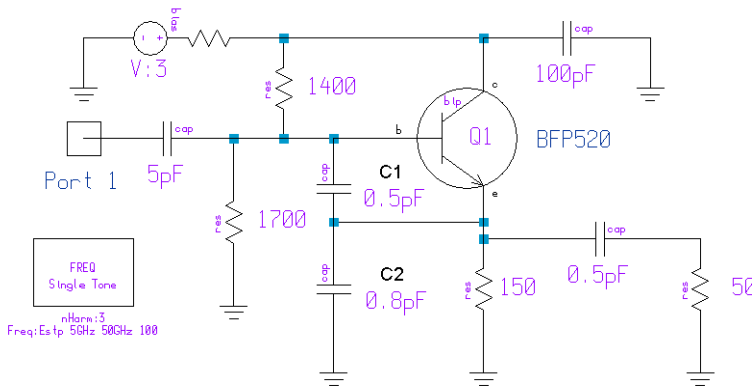


Figure 4--Test circuit for simulation purposes. By analyzing Z_{11} as a function of frequency, one can determine the available frequency range of oscillation for a given set of capacitors (C_1 [0.5 pF], C_2 [0.8 pF]) and as a function of dc bias.

The capacitors C_1 and C_2 , which were mentioned in (1), are 0.5 pF and 0.8 pF in Figure 3, plus the intrinsic capacitance of the transistor. To be specific, base-emitter junction and diffusion capacitances are in parallel with C_1 and the collector-emitter capacitance is in parallel with C_2 . To get output from the oscillator, we used a coupling capacitor from the emitter as seen in Figure 4, as well as a capacitive voltage divider as part of the resonator as shown in Figure 5. The actual resonating frequency, which is determined by the reactive elements, can be approximated from Figure 6, which graphs the real and imaginary portions of the test current applied to the circuit by the Oscillator Design Aid in the Serenade Design Environment. This is equivalent to the negative resistance of (1), which then drives a negative current to compensate the losses. Besides finding the actual resonance frequency, we see that there is sufficient loop gain to tune the oscillator up to about 23 GHz, the crossover point for the real component of the test current becoming positive again.

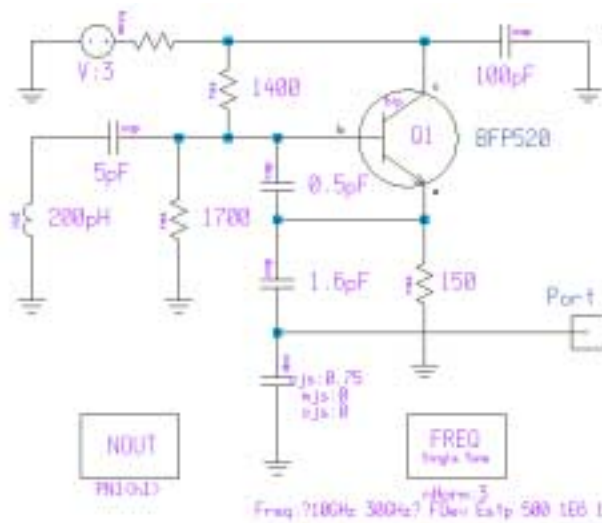


Figure 5--The complete Colpitts oscillator using a 45-GHz transistor. It oscillates at 17 GHz. To evaluate the difference in noise performance, we took the output as part of the tuned circuit at the capacitive voltage divider and directly from the emitter (see Figure 10).

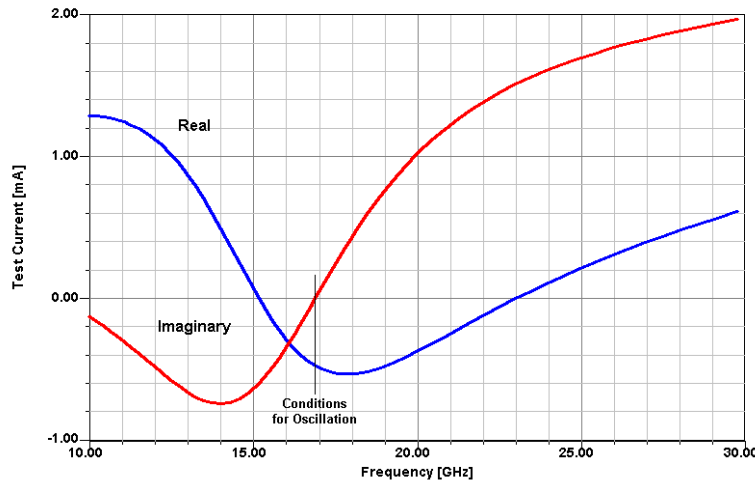


Figure 6--The oscillation frequency is determined by the crossover point of the reactance from capacitive to inductive (imaginary part of test current = 0) and the real portion must be negative and large enough to compensate the resonator losses.

The oscillator circuit (Figure 5) is biased at about 4 mA and operates at 3 V. One of the problems with these microwave transistors is that they only tolerate fairly low voltages, and one needs to make sure that the voltage swing across the transistor does not exceed certain values (breakdown voltage).

Low-noise operation also requires a low dc current compared to the maximum allowed current. In this device, the maximum current is around 35 mA, but the 4 mA operating point results in a lower flicker corner frequency. Figure 7 shows the bias-dependent measured transition frequency (f_T), which is a strong function of the current, as can be seen. In the case of our 4 mA operating point, the resulting f_T is somewhere around 25 GHz. f_T is defined as

$$f_T = \frac{1}{2\pi C_E R_D} \quad (2)$$

with

$$R_D = \frac{26 \text{ mV}}{I_E} \quad (3)$$

and

$$C_E = \frac{w^2 I_E}{2D V_T} \quad (4)$$

where I_E = emitter current, R_D = emitter diffusion resistance, C_E = emitter diffusion capacitance, w = effective base width, D = diffusion constant for the transistor, and $V_T = 26 \text{ mV}$. This equation implies that f_T is constant, since the current cancels in the denominator. However, this equation is not reciprocal, meaning that once we know the emitter diffusion resistance and its capacitance, we can calculate f_T but the bias changes apparently modulate w and therefore the equation for C_D does not hold below 20 mA. In other words, most of the nonlinearity is concentrated in the emitter diffusion capacitance, which is responsible for the steep changes.

Transition Frequency
 versus Collector Current
 $f = 2 \text{ GHz}$

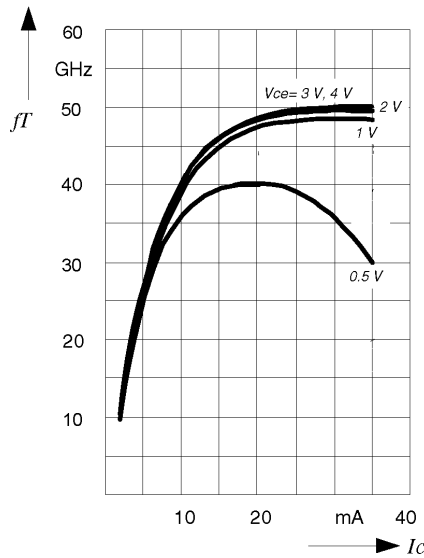


Figure 7--Bias-dependent transition frequency f_T measured at 2 GHz by monitoring the frequency-dependent current gain. For low-noise operation, one typically sets a bias point in the middle of the curve (for example, 5 mA), which unfortunately results in a highly nonlinear relationship between phase noise and collector current.

Figure 8 shows the dc I - V curve with the load line included. A typical load line for an RC amplifier is a straight line; the very moment a tuned circuit, which stores energy, is included, the load line changes into a closed load curve, the area of which is related to the dynamic changes of the reactances of the device. The load line also gives insight into such effects as reverse currents, where the collector-base voltage approaches the breakdown value and the base takes some of the current. It also indicates that the L - C ratio is too low for the impedance, as we see a high change in current but a low change in voltage. On the other hand, this loose coupling maintains a high Q .

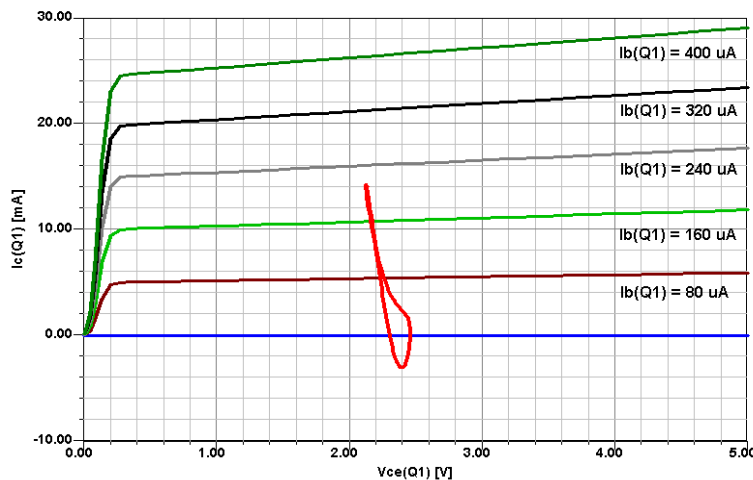


Figure 8--DC I - V curve of the Colpitts oscillator. The load line exhibits not much of an expanded area, which means that the transistor is run fairly linearly. The lower section of the curve, which opens, reflects energy stored in the base-emitter junction.

Another nonlinear effect that deals with loading is the output spectrum of the oscillator. In most cases, the first harmonic is suppressed by about 20 dB. This is shown in Figure 9.

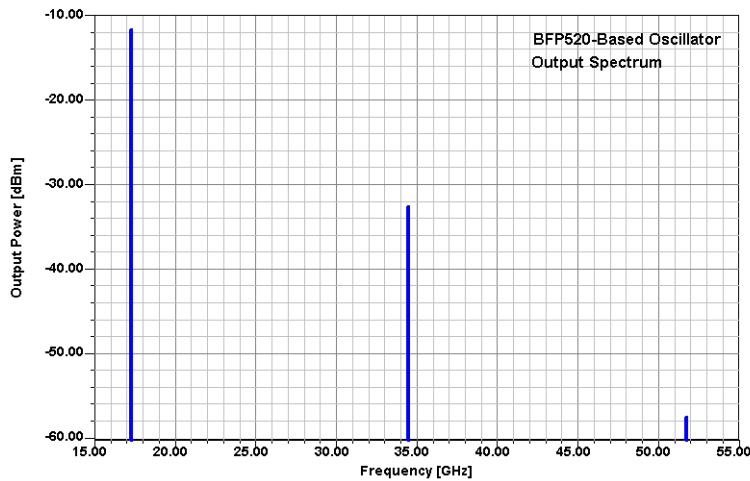


Figure 9--Predicted output spectrum for the Colpitts oscillator operating around 17 GHz. The resonator helps to clean up the unwanted harmonics. The resonator's operating Q must be fairly high to achieve this level of harmonic suppression.

Returning to the question of the output coupling and now evaluating the phase noise of the oscillator, we obtain the values shown in Figure 10. Because of the filter effect of the capacitive voltage divider, the far-out noise performance gets better as a function of frequency. A point can be made that it's always a bad choice to take the output directly from the emitter or collector because it contains more wideband noise and loads the circuit more heavily.

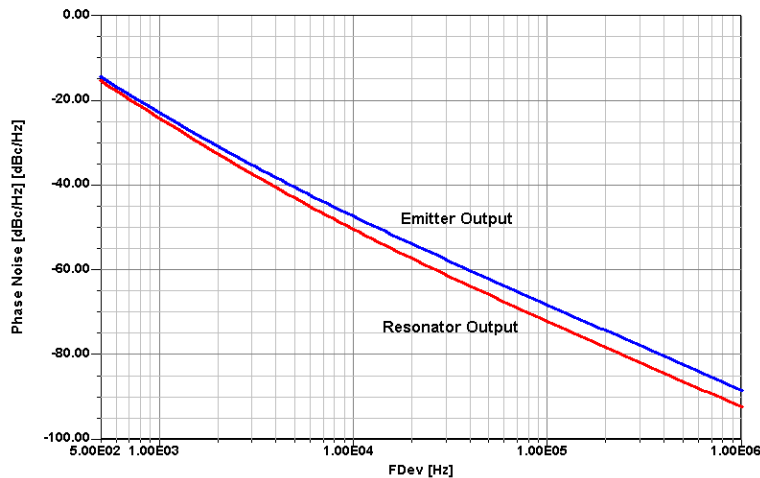


Figure 10--Taking the output from a part of the resonator provides better phase noise performance than either the emitter or collector current will supply into a termination. If possible, one should use an isolation amplifier with a high input impedance to minimize loading of the tuned circuit.

Noise is related to linear operation but then gets superimposed on the carrier of an oscillator by the inherent nonlinearities of the device.

Introduction to Phase Noise

Phase noise is defined as the ratio of the peak carrier signal to the noise at a specific offset off the carrier expressed in dB below the carrier in a 1-Hz bandwidth. Since most measurements done are in a wider bandwidth, the correction factor is

$$C = 10 \log(B) \quad (5)$$

where C is the correction factor and B is the bandwidth. For 1 kHz, $C = 30$ dB. Relative to 0 dBm (1 mW), the best phase noise obtainable at 300 kelvins is -174 dBc/Hz.

The phase noise of a voltage-controlled oscillator (VCO) is determined by [11, pp. 93-98]

$$\mathcal{L}(f_m) = 10 \log \left\{ \left[1 + \frac{f_0^2}{(2f_m Q_{load})^2} \right] \left[\left(1 + \frac{f_c}{f_m} \right) \frac{FkT}{2P_{sav}} + \frac{2kTRK_0^2}{f_m^2} \right] \right\} \quad (6)$$

where

$\mathcal{L}(f_m)$ = ratio of sideband power in 1-Hz bandwidth at f_m to total power in dB

f_m = frequency offset

f_0 = center frequency

f_c = flicker frequency

Q_{load} = loaded Q of the tuned circuit

F = noise factor

$kT = 4.1 \times 10^{-21}$ at 300 K (room temperature)

P_{sav} = average power at oscillator output

R = equivalent noise resistance of tuning diode

K_0 = oscillator voltage gain

When adding an isolating amplifier the noise of an IC oscillator is determined by

$$\begin{aligned} S_{\phi}(f_m) = & \left[a_R F_0^4 + a_E (F_0 / (2Q_L))^2 \right] / f_m^3 \\ & + \left[(2GFkT / P_0) (F_0 / (2Q_L))^2 \right] / f_m^2 \\ & + (2a_R Q_L F_0^3) / f_m^2 \\ & + a_E / f_m + 2GFkT / P_0 \end{aligned} \quad (7)$$

where

G = compressed power gain of the loop amplifier

F = noise factor of the loop amplifier

K = Boltzmann's constant

T = temperature in kelvins

P_0 = carrier power level (in watts) at the output of the loop amplifier

F_0 = carrier frequency in Hz

f_m = carrier offset frequency in Hz

$Q_L (= \pi F_0 \tau_g)$ = loaded Q of the resonator in the feedback loop

a_R and a_E = flicker noise constants for the resonator and loop amplifier, respectively

While this refers to a VCO, any oscillator already shows a voltage- and current-dependent frequency. This characteristic whereby a change of the voltage (supply voltage in this case) is called *pushing*. It is expressed in kilohertz or megahertz per volt. All active devices have voltage- or current-dependent capacitances that are responsible for voltage-dependent frequency shifts. One can "take the internal capacitance out" and make them concentrated in one external device, such as a tuning diode. The left part of (6) is the oscillator term with the flicker noise added, while the last term is responsible for the modulation noise. We define the modulation noise as the noise that is generated by actually modulating the oscillator. Any noise source in

series with the tuning diode will cause a frequency modulation, which is translated into phase noise. There is an additional phenomenon called *conversion noise*, which is produced in a manner similar to mixing. This noise portion is responsible for the far-out noise. The following section gives some insight into the nonlinear effects responsible for the noise contribution to the oscillator signal.

Nonlinear Effects Responsible for Noise in Oscillators

The following assumptions are made for an oscillator. The circuit supports a large-signal time-periodic autonomous regime. The circuit is perturbed by a set of small sources located at the carrier harmonics and at the sidebands at a deviation ω from carrier harmonics.

Now we can find the results of the perturbation of the harmonic-balance equations. The perturbation of the circuit state ($\delta X_B, \delta X_H$) is given by the uncoupled sets of equations

$$\frac{\partial E_B}{\partial X_B} \delta X_B = J_B(\omega) \quad (8)$$

$$\frac{\partial E_H}{\partial X_H} \delta X_H = J_H(\omega) \quad (9)$$

where

E_B, E_H = vectors of harmonic-balance errors

X_B, X_H = vectors of state-variable (SV) harmonics (since the circuit is autonomous, one of the entries of X_H is replaced by the fundamental frequency ω_0)

J_B, J_H = vectors of forcing terms where the subscripts B and H denote sidebands and carrier harmonics, respectively

Conversion and Modulation Noise. For a spot noise analysis at a frequency deviation ω , the noise sources can be interpreted in either of two ways. For pseudo-sinusoids with random amplitude and phase located at the sidebands, noise generation is described by (8), which is essentially a frequency-conversion equation relating the sideband harmonics of the state variables and of the noise sources. This description is exactly equivalent to the one provided by the frequency-conversion approach. The mechanism is referred to as *conversion noise*. For sinusoids located at the carrier harmonics, randomly phase- and amplitude-modulated by pseudo-sinusoidal noise at frequency ω , noise generation is described by (9), which gives the noise-induced jitter of the circuit state, represented by the vector δX_H . The modulated perturbing signals are represented by replacing entries J_H with the complex modulation laws. This mechanism is referred to as *modulation noise*.

Properties of Modulation Noise. One of the entries in δX_H is $\delta\omega_0$. $\delta\omega_0(\omega)$ equals the phasor of the pseudo-sinusoidal components of the fundamental frequency fluctuations in a 1-Hz band at frequency ω . (10) provides a frequency jitter with a mean square value proportional to the available noise power. In the presence of both thermal and flicker noise sources, PM noise increases as ω^{-3} for $\omega \rightarrow 0$ and tends to 0 for $\omega \rightarrow \infty$. Modulation-noise analysis correctly describes the noise behavior of an oscillator at low deviations from the carrier frequency but

does not provide results consistent with physical observations at high deviations from the carrier frequency.

Noise Analysis of Autonomous Circuits. Conversion noise and modulation noise represent complementary descriptions of noise generation in autonomous circuits. The previous discussion has shown the very-near-carrier noise is essentially a modulation phenomenon, while very-far-from-carrier noise is essentially a conversion phenomenon; also, (8) and (9) necessarily yield the same evaluation of PM noise at some crossover frequency ω_X . The computation of PM noise should be performed by modulation analysis below ω_X and by conversion analysis above ω_X .

This criterion is not artificial since (8) and (9) provide virtually identical results in a wide neighborhood of ω_X (usually more than two decades). The same criterion can be applied to AM noise. (In many practical cases, modulation and conversion analyses yield almost identical AM noise at all frequency deviations.)

Conversion Noise Analysis Results. After performing all the necessary calculations, we obtain the following:

- k th harmonic PM noise

$$\langle |\Phi_k(\omega)|^2 \rangle = \frac{N_k(\omega) + N_{-k}(\omega) - 2\text{Re}[C_k(\omega)]}{R|I_k^{SS}|^2} \quad (10)$$

- k th harmonic AM noise

$$\langle |\delta A_k(\omega)|^2 \rangle = 2 \frac{N_k(\omega) + N_{-k}(\omega) + 2\text{Re}[C_k(\omega)]}{R|I_k^{SS}|^2} \quad (11)$$

- k th harmonic PM-AM correlation coefficient

$$\begin{aligned} C_k^{\text{PM-AM}}(\omega) &= \langle \delta \Phi_k(\omega) \delta A_k(\omega)^* \rangle \\ &= -\sqrt{2} \frac{2\text{Im}[C_k(\omega)] + j[N_k(\omega) - N_{-k}(\omega)]}{R|I_k^{SS}|^2} \end{aligned} \quad (12)$$

where

$N_k(\omega)$, $N_{-k}(\omega)$ = normalized correlation coefficient of the upper and lower sidebands of the k th carrier harmonic

R = load resistance

I_k^{SS} = k th harmonic of the steady-state current through the load

Modulation Noise Analysis Results. Again, after performing all the necessary calculations, we obtain the following:

- k th harmonic PM noise

$$\langle |\delta\Phi_k(\omega)|^2 \rangle = \frac{k^2}{\omega^2} T_F \langle J_H(\omega) J_H^t(\omega) \rangle T_F^t \quad (13)$$

- k th harmonic AM noise

$$\langle |\delta A_k(\omega)|^2 \rangle = \frac{2}{|I_k^{SS}|^2} T_{Ak} \langle J_H(\omega) J_H^t(\omega) \rangle T_{Ak}^t \quad (14)$$

- k th harmonic PM-AM correlation coefficient

$$\begin{aligned} C_k^{\text{PM-AM}}(\omega) &= \langle \delta\Phi_k(\omega) \delta A_k(\omega)^* \rangle \\ &= \frac{k\sqrt{2}}{j\omega |I_k^{SS}|^2} T_F \langle J_H(\omega) J_H^t(\omega) \rangle T_{Ak}^t \end{aligned} \quad (15)$$

where

- $J_H(\omega)$ = vector of Norton equivalent of the noise sources
- T_F = frequency transfer matrix
- T_{Ak} = amplitude transfer matrix
- R = load resistance
- I_k^{SS} = k th harmonic of the steady-state current through the load

The Ceramic-Resonator-Based Oscillator (CRO)

It is fairly difficult to build high- Q resonator circuits at the frequency range above 500 MHz. Printed circuit board implementations are lossy, and radiate a lot. Also, they are microphonic. A better choice is a resonator like a rigid cable, which is based on a piece of ceramic that is silver-plated, looks like a small tube, and has one end electrically short-circuited. Since values of ϵ_r from 38 to 88 are available in high-performance ceramics, the actual physical size of the ceramic resonator becomes very small, resulting in a very low impedance (low L - C ratio). In the case of $\epsilon_r = 88$ material, the required length in millimeters is $8.2/f$, leading to a significant reduction in physical length. The obtainable Q is in the vicinity of 400. For smaller ϵ_r values, the Q will go up to 800. Figure 11 shows a photograph of a typical CRO. Its schematic is not much different from the Colpitts oscillator, as can be seen in Figure 12.

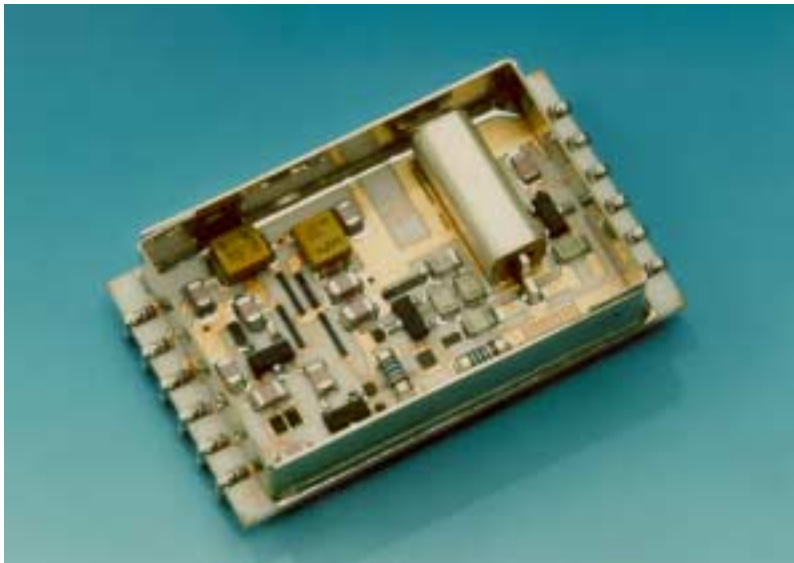


Figure 11--Photo of a ceramic-resonator-based oscillator.

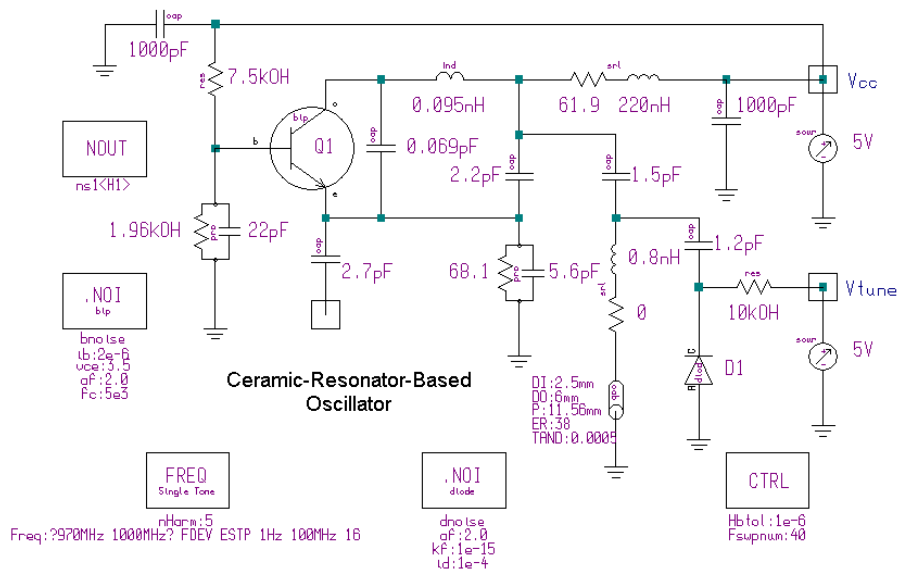


Figure 12--Typical ceramic-resonator-based oscillator. It may be of interest to know that most of the far-out noise comes from the tuning diode and is not related to the Q of the resonator. This is a frequently misunderstood fact. This noise contribution is also not due to the Q of the diode, but to its inherent equivalent noise resistance. Reducing the value of the 10-k Ω resistor in the diode's V_{tune} line will further reduce the noise contributed by the diode portion of the circuit to that produced by the diode itself.

This oscillator circuit is similar to the Clapp oscillator. It operates in the grounded-base configuration, and the feedback is formed by the 2.2-pF capacitor between the collector and emitter, and the 5.6-pF capacitor between the emitter and ground. The 900-MHz resonator is coupled to the oscillator with 1.5 pF, and a tuning diode with 1.2 pF. The ceramic resonator is about 11 mm long and 6 mm in diameter, and the ϵ_r is 38, resulting in an unloaded Q of 500. Because this type of oscillator is mostly operated between 500 MHz and 2 GHz, the base grounding capacitor is very critical. Since the values of the feedback capacitances are fairly high, taking the output from the emitter is tolerable; a better way would have been to split the 5.6-pF capacitor into two series-connected values that give the same amount of coupling.

Now we want to see whether the oscillator will actually "take off," and the picture of the test current components (Figure 13) shows that the crossover point for the imaginary component of the test current is at 982 MHz, but the real current stays negative up to about 990 MHz, so the oscillator can be tuned over a wider range.

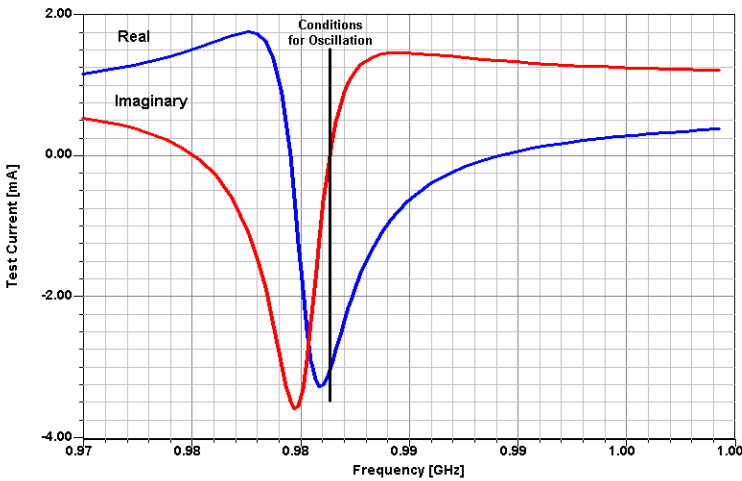


Figure 13--The steepness of the curve showing the test currents indicates a high operating Q that results in low phase noise. The steeper the slope at the changeover from inductive to capacitive reactance, the higher the resonator Q .

Since we are using a high- Q oscillator, we can expect very good phase-noise performance, as the simulated phase-noise curve of Figure 14 shows. The curve also shows the breakpoint for the flicker noise. We measured the actual oscillator and found that the difference between simulation and measurement was less than 2 dB. This is valid from 100 Hz from the carrier to 10 MHz off the carrier. At frequency offsets greater than this, the measurement becomes quite difficult.

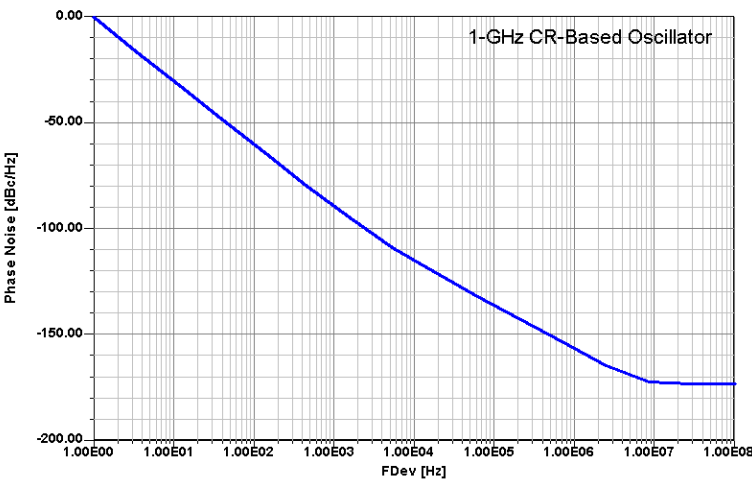


Figure 14--SSB phase of a typical ceramic-resonator-based oscillator operating around 900 MHz. The breakpoint at about 5 kHz is due to the transistor's flicker noise contribution. The ultimate phase noise (breakpoint near 10 MHz) is due to KT_0 (-174 dBc/Hz).

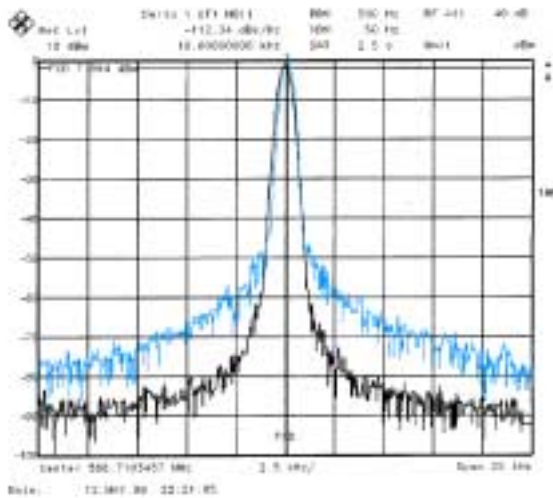


Figure 14a--shows the phase noise improvement caused by the novel RFIC oscillator circuit, which includes a tuning diode. However, the tuning diode coupling is only about 10MHz per volt, and therefore, does not add to the modulation noise. For test purposes, this is an LC circuit with a loaded Q of 50 measured at about 500MHz. The IC operates up to 3GHz.

Further Improvements

The CR-based oscillator has shown an extremely good phase noise due to the high- Q resonator. We also saw that the flicker noise became quite apparent as a limitation for the close-in phase noise. A way around this is to use a feedback circuit with two functions: (1) It stabilizes collector/emitter current of the transistor; (2) it also samples all the noise from dc to about 1 MHz off the carrier and feeds these components back into the base of the oscillator transistor with a phase shift of 180° . Inside the loop bandwidth of this feedback circuit, shown in Figure 15, the phase noise is drastically improved. The same can be achieved with a *pnp* transistor sampling the collector current with the emitter of the transistor at dc ground. This circuit has been used for years but nobody seems to have realized that by using the appropriate R - C time constants it can be used as such an anti-noise feedback circuit.

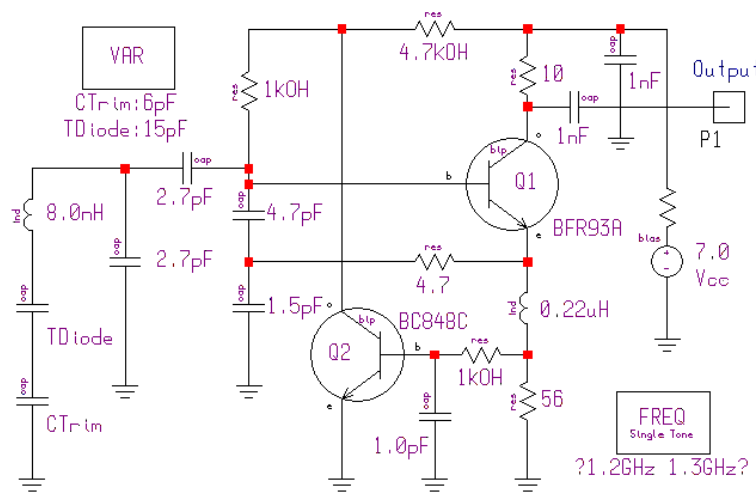


Figure 15--Modified Colpitts oscillator with a dc-stabilizing circuit that monitors the emitter current of the oscillator transistor. Since the stabilizing transistor is dc-coupled, it can be used as a feedback circuit to reduce the phase noise from dc to about 1 MHz off the carrier. This approach is independent of the operating frequency and the device itself, and therefore can be used for FETs as well as bipolar transistors. It solves the f_T nonlinearities pointed out in Figure 7.

A Lumped Resonator Oscillator (LRO)

A popular circuit for actually building DROs is shown in Figure 16. By adding a base inductor of several hundred picohenrys, the transistor will become highly unstable. When varying the base inductance, S_{11} (1-port relative to the collector, expressed in dB) becomes increasingly positive and larger than 1 (Figure 17). The tuned circuit at the emitter generates a maximum for S_{11} as the capacitance is changed in value (Figure 18). For a given set of parameters, the frequently used test current (as indicated by the Oscillator Design Aid, part of Ansoft's Serenade Design Environment) shows conditions for resonance slightly above 10 GHz (Figure 19). The Design Aid performs a nonlinear calculation and takes some of the parameter changes of the transistor into consideration. This explains the difference between the resonance frequency predicted by the Design Aid and that determined by a full harmonic-balance calculation.

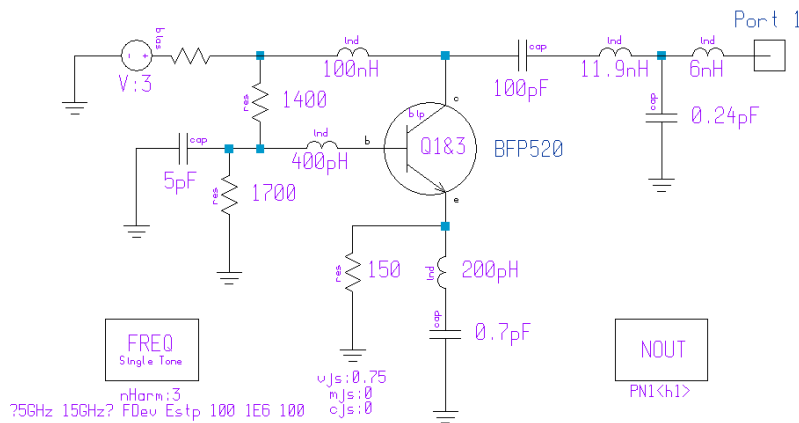


Figure 16--Schematic of a Clapp-Gouriet-based lumped-resonator oscillator (LRO), including a collector matching network. This is a very popular circuit when used with dielectric resonators, which are placed in the emitter circuit, coupled to a transmission line. Changes at the collector, base, and emitter of the circuit have a strong effect on the resonant frequency for the LRO type. Even the DRO will show a soft response as to frequency changes as a function of load shifts (capacitive and resistive).

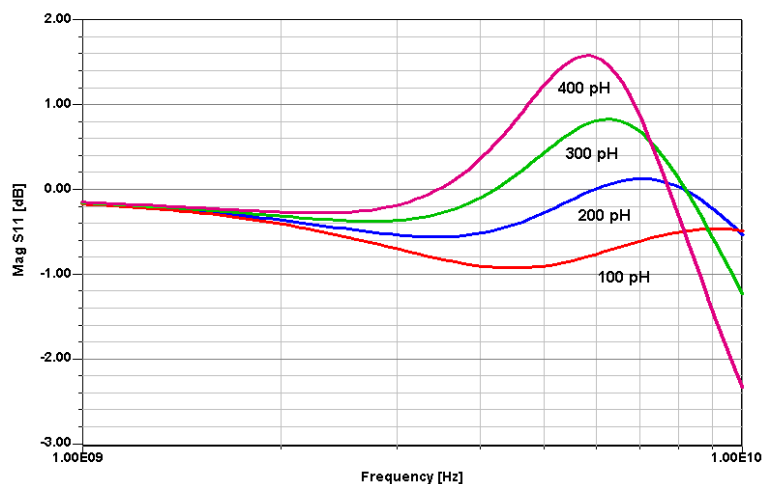


Figure 17--Effect of varying the LRO base inductance as indicated by the magnitude of S_{11} , expressed in dB, looking into the oscillator output port (collector). An initial value of 400 pH was necessary to generate the sufficiently high negative resistance that is a prerequisite for oscillation startup. To complicate life, we will find that because the base and emitter circuits are highly interactive, there is therefore no single, unique set of base and emitter component values that will support oscillation at a given frequency.

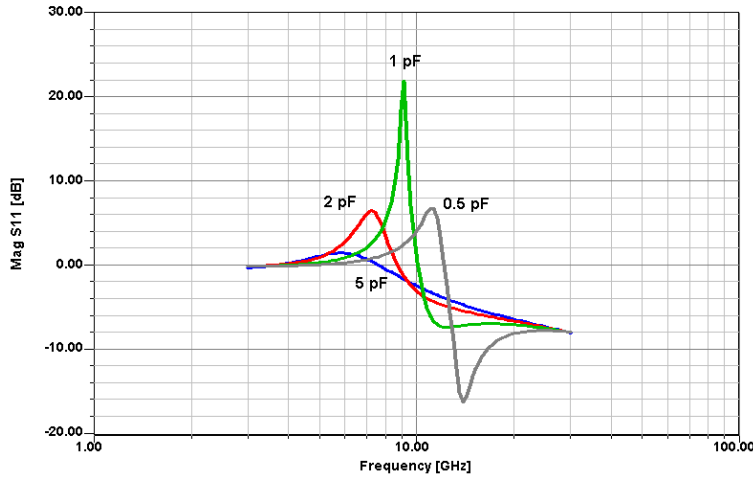


Figure 18--Effect of varying the emitter capacitance of the LRO as indicated by the magnitude of S_{11} , expressed in dB, looking into the oscillator output port (collector). A value of about 20 dB is needed to guarantee oscillation startup at the desired frequency of about 10 GHz.

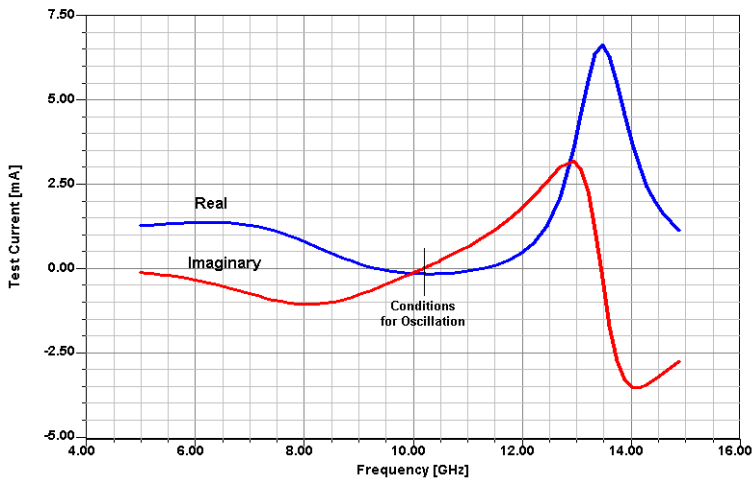


Figure 19--Display of the test currents for the LRO circuit. The imaginary curve is fairly shallow, indicating medium resonator Q . A steeper resonance, but no negative resistance, can be seen around 14 GHz; an optimized design would move this portion toward the desired oscillation frequency (10 GHz).

It has been mentioned that it was difficult to obtain reliable data on the silicon-germanium (SiGe) transistor suitable for this type of operation. In order to study the influence of the various components of the transistor on the phase noise, we started off using a fairly simplified model. We then successively added all the dc parameters and internal losses such as emitter and collector loss resistances, and finally--resulting in a big jump in phase--the base spreading resistance. It becomes obvious that the base spreading resistance adds the most dramatic change to the phase noise as reflected in Figure 20. The difference is practically 15 dB. It would be nice to be able to build microwave transistors with base spreading resistances much less than 8 Ω .

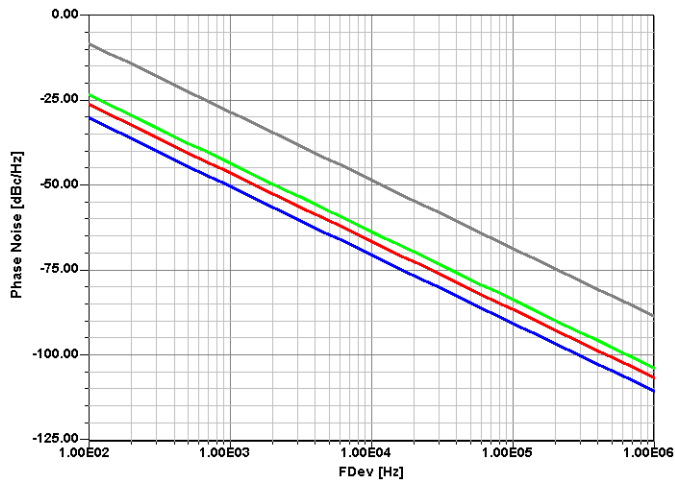


Figure 20--Phase noise prediction of the modified Colpitts oscillator as a function of the transistor model. Starting with the most simple device model, we successively added internal losses and finally the base spreading resistance, which shows the greatest jump towards worse phase noise. This was necessary to validate certain commercially used models.

Taking the power from the collector is always an adventure because of the unwanted pushing and the wideband noise floor. However, if the matching network in the collector reduces the load on the collector, than the phase noise can still be improved. This is obvious in Figure 21. If the output has to be taken at the collector, the matching network really cleans up the phase noise.

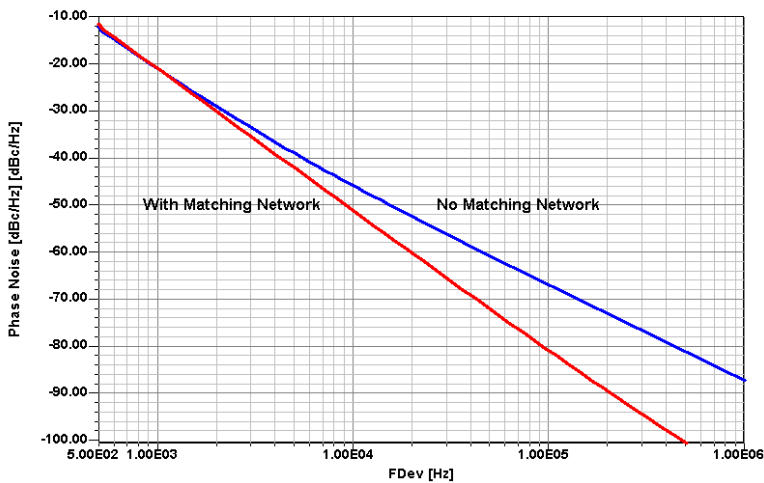


Figure 21--By using a matching network at the collector rather than taking the energy directly from it, the phase noise can be improved. The reason for this is that the matching network provides a better termination at the collector, and therefore minimizes the effect of the collector-emitter and collector-base (Miller effect) capacitances. In addition, we get more output power.

The better matching also results in more output power; this can be observed in Figure 22. An interesting side-effect is that the added reactances push the frequency down significantly--almost to half of the starting frequency. This is one of the reasons why having the emitter, base, and collector electrically hot is very dangerous; everything now interacts. We do obtain more output power and the phase noise is better, but we would have to change the tuned circuit to regain our higher desired oscillation frequency. This is a typical case where a linear simulator using measured S parameters at one bias point will fail.

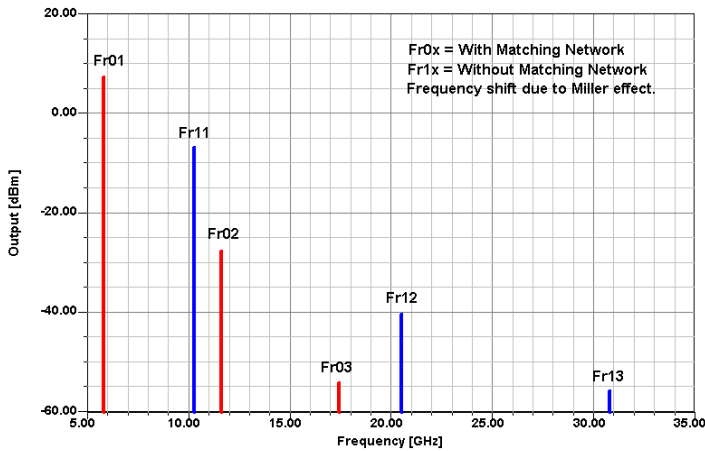


Figure 22--Output spectrum for the LRO with and without an output matching network. While adding the output network increased the output power, the operating frequency also jumped significantly down. It needs to be optimized to get additional harmonic suppression while maintaining the fundamental output.

Low Phase Noise Sources

In many cases, it is necessary to stabilize the oscillators in the sense that we make them part of a phase locked loop which results in a microwave synthesizer. Figure 23 shows a VCXO oscillating at 100MHz. Its predicted phase noise can be seen in Figure 24. This oscillator is actually used in a variety of Rohde & Schwarz signal generators and can be phase locked against a primary or secondary frequency standard.

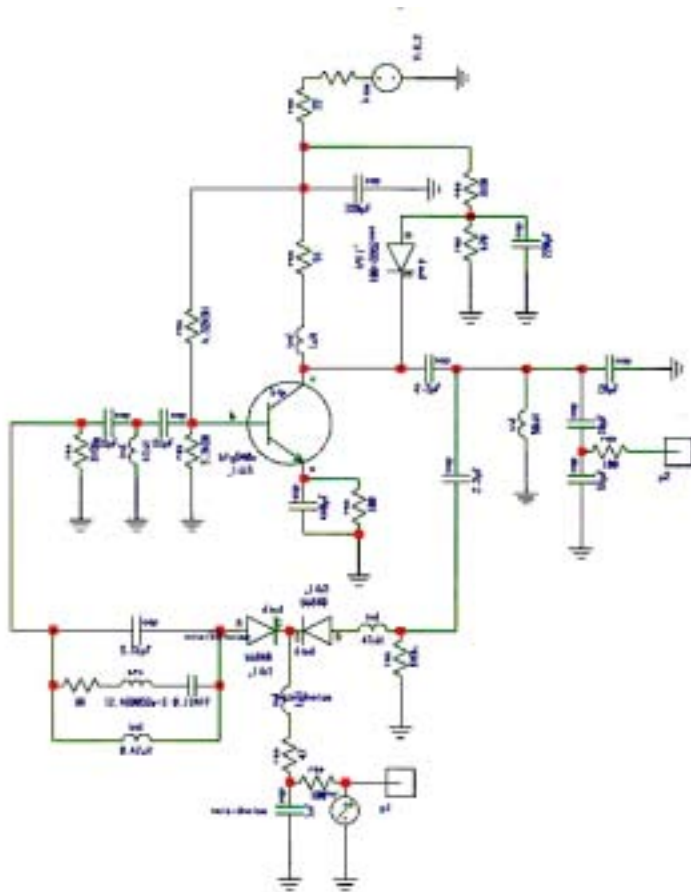


Figure 23-- Low phase 100MHz noise crystal reference oscillator using limiting diode to improve performance.

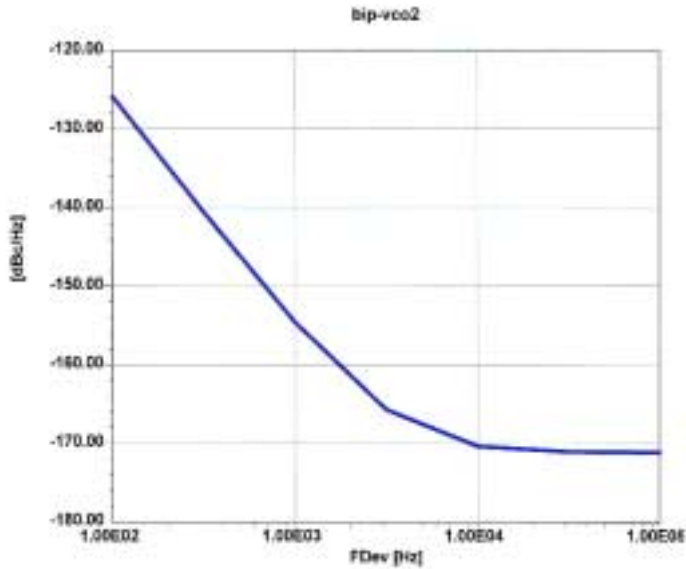


Figure 24-- Predicted phase noise of the previous crystal oscillator.

Moving to Distributed Elements

So far, we have designed oscillators using inductances, and we really did not take into consideration whether their values are feasible or if they had a reasonable Q . It is not a good assumption to consider a bond wire to be a high- Q resonator--and yet, some of the inductances can become so small that the bond wire plays a considerable role. For microwave applications, transistors have to be either in chip form or have to be part of the integrated circuit; in these cases, these parasitic elements do not exist. An inductance can be replaced by a microstrip element that is shorter than the length required for $\lambda/4$ resonance. Figure 25 shows that the steepness of the reactance curve of a transmission line close to resonance is much more pronounced than that of an inductance.

We had previously examined the influence of biasing on the phase noise, so we thought it a good idea to show the impact of bias and resonator type on phase noise. Figure 25 shows this, as well as the phase noise as a function of constant-current versus constant-voltage biasing.

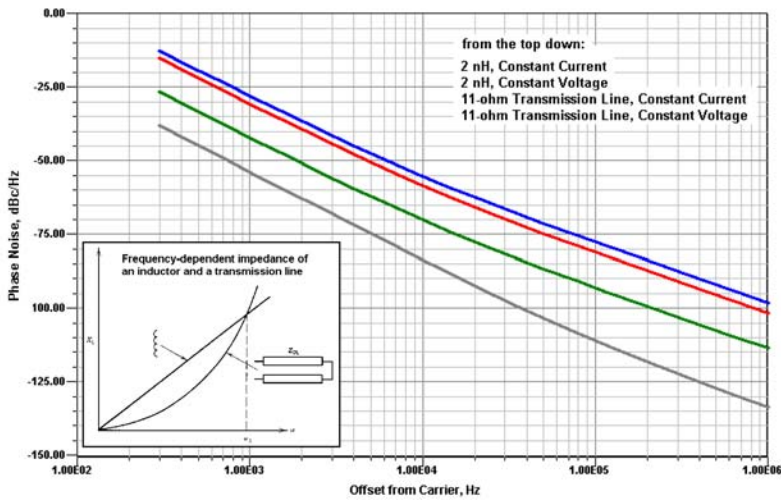


Figure 25--Transistor oscillators are sensitive to the bias network and to the resonator circuit. As a test we have differentiated constant-current and constant-voltage biasing, as well as interchanging inductors with transmission lines. The phase noise improves with the use of a transmission line and a constant-voltage bias source. (A constant-voltage source prevents a dc bias shift. The dual of a constant voltage at the base is a constant-current source at the emitter.)

A popular resonator for microwave applications is a dielectric resonator as shown in Figure 26. This type of resonator can be modeled by using a physical model such as found in the Ansoft Serenade linear/nonlinear simulator.

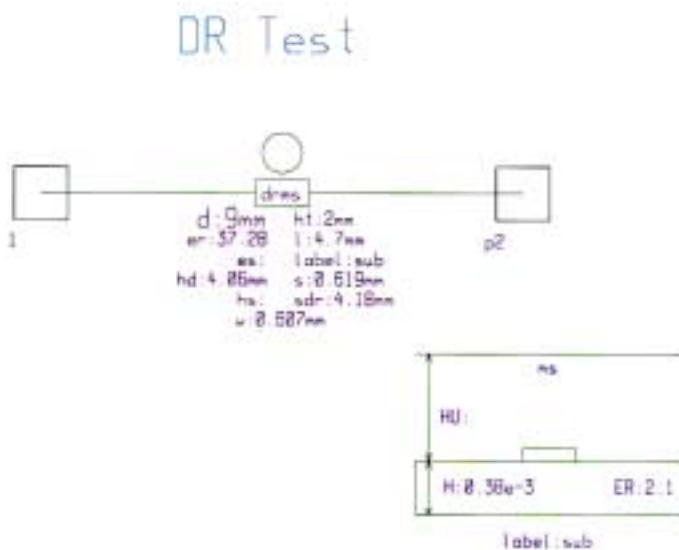


Figure 26-- Physical model of dielectric resonator.

An actual oscillator using a feedback RF choke in the base is shown in Figure 27. It needs to be noted that these type of oscillators are both very temperature sensitive and the resonant frequency can be easily altered by changing the cover above the DR. It is advisable that these oscillators get locked against a primary or secondary standard for better frequency stability. This technique can be extended easily up to 18GHz.

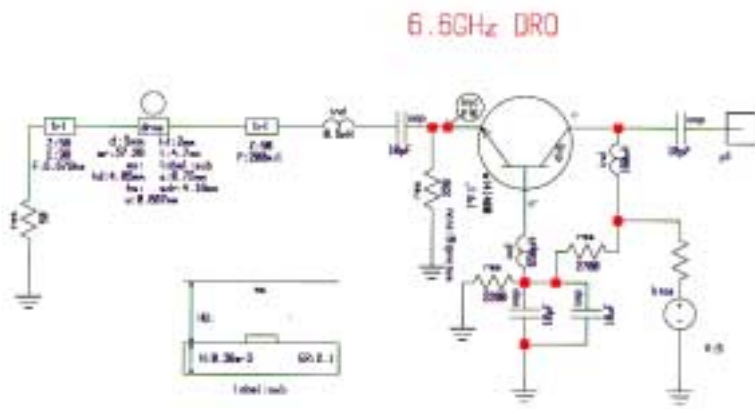


Figure 27--Dielectric-based oscillator at about 6.6GHz.

Figure 28 shows the schematic of such a resonator-based oscillator. However, here a parallel equivalent circuit has been used for modeling purposes. To determine the oscillator frequency we can use the design tool of the Serenade simulator as shown in the introduction. For oscillation, we require a negative resistance, and at the same time the imaginary currents have to go through 0. The crossover point for the linear simulator occurs at 18.53GHz of Figure 29.

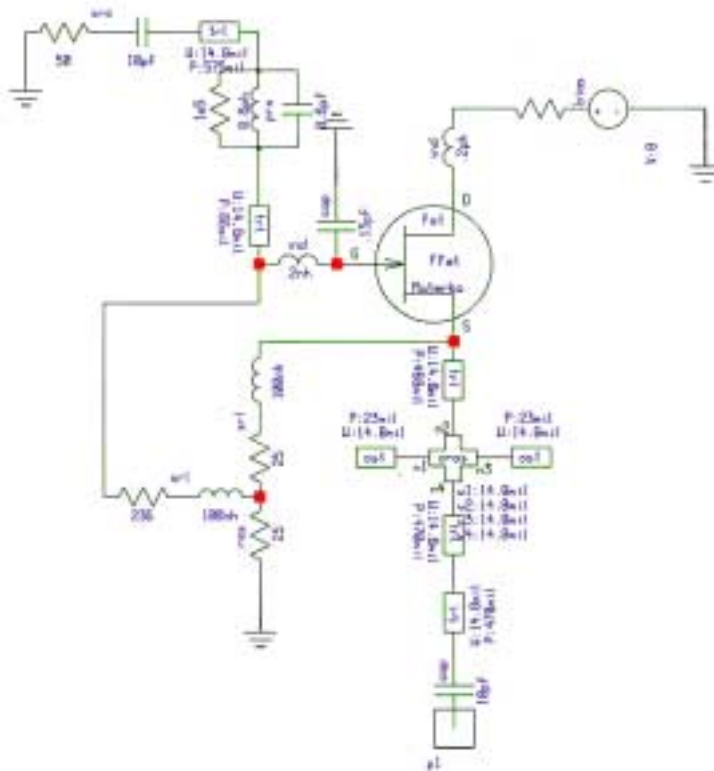


Figure 28--18GHz dielectric resonator oscillator.

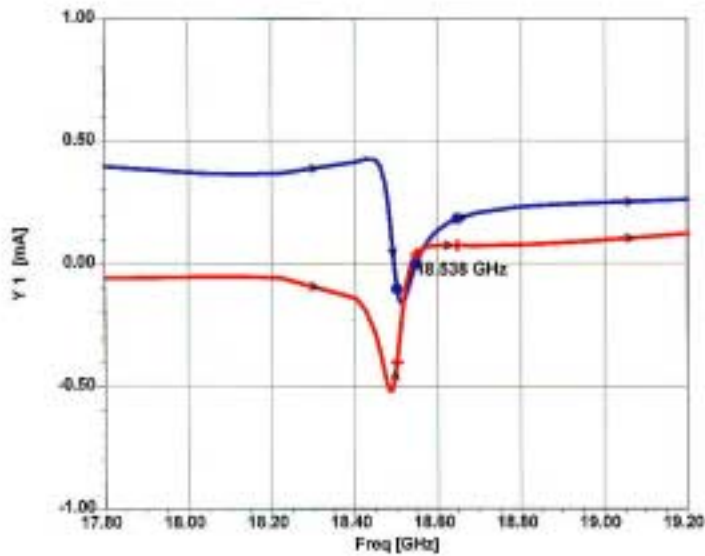


Figure 29--Determination of exact oscillating frequency of the oscillator.

Many authors have claimed that the use of linear S parameters or a linearized model is adequate method to determine the oscillation frequency exactly, however, this is a poor assumption. In all cases where the intrinsic capacitance of the transistor determines the oscillator frequency, the large signal biasing can shift the frequency as much as 10%, typically, to a lower frequency for bipolar transistors and a higher frequency with FETs. Unfortunately, this is a somewhat politically motivated statement by authors who avoid the higher costs of a good harmonic-balanced simulator. This initially higher investment pays off rapidly because it does not only predicted proper phase noise information, but also accurate output levels. These can be easily seen in Figures 30 and 31. It may be useful to show that these nonlinear simulators can also predicted the noise analysis for a mixer.

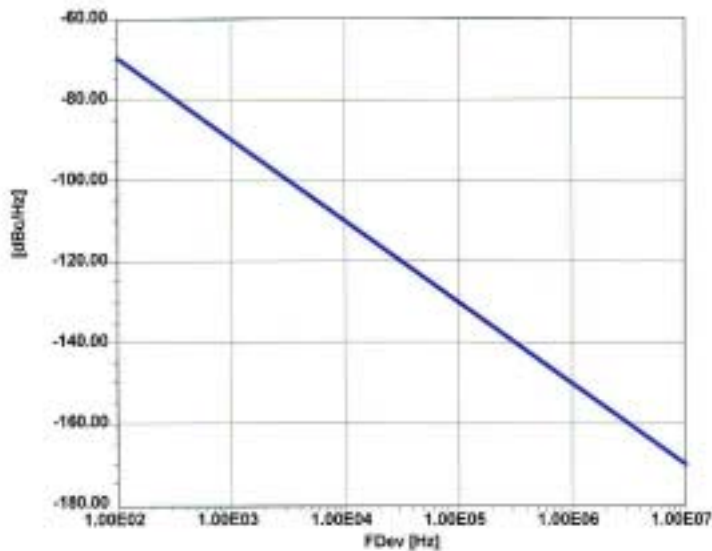


Figure 30--Predicted phase noise of the 18GHz DRO.

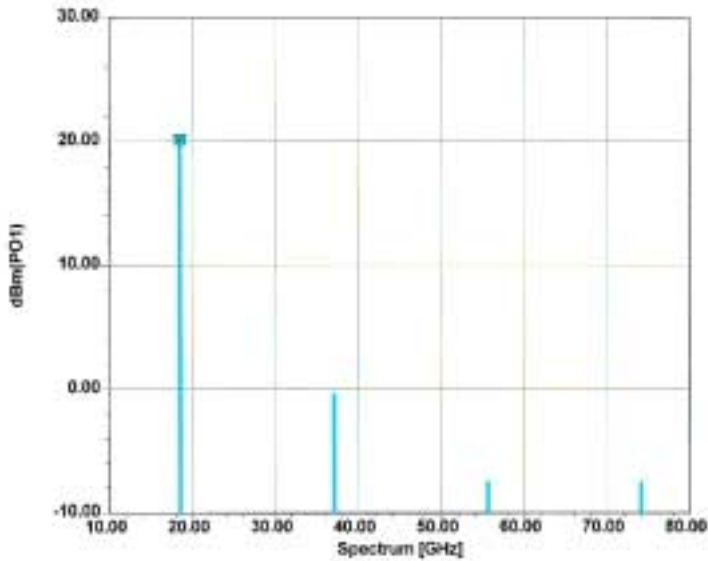


Figure 31--Predicted output spectrum of the DRO.

Figure 32 shows the circuit arrangement which is a combination of an oscillator and a mixer. These circuits are called self-oscillating mixers. Generally, they are not very popular because of pulling effects, but for low-cost applications, they need to be considered. After slight modifications, a similar topology in Figure 33 shows a standard mixer at microwave frequencies.

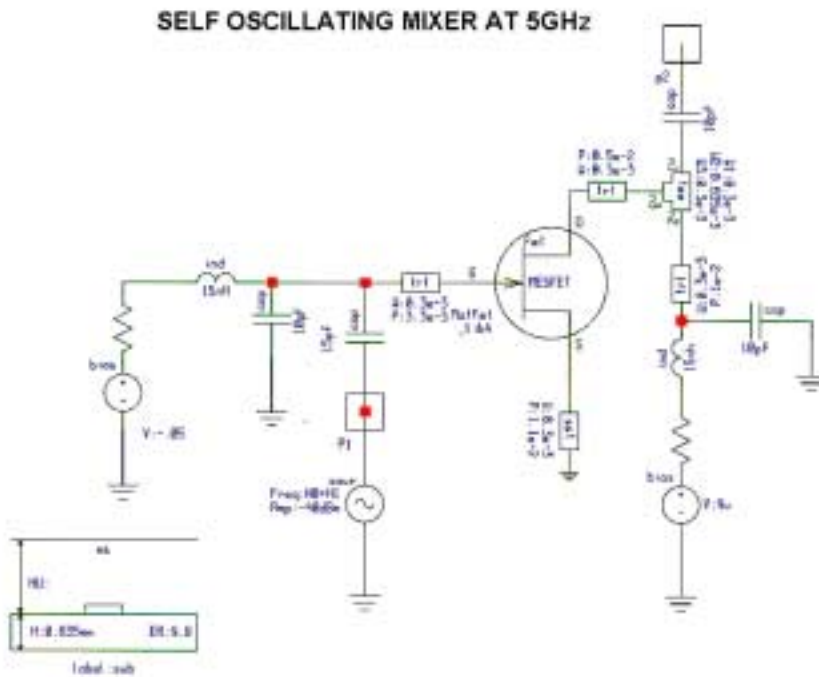


Figure 32--Combination of an oscillator and mixer. The IF is taken off the drain circuit.

Nonlinear Noise Analysis of a Single Gate FET Mixer

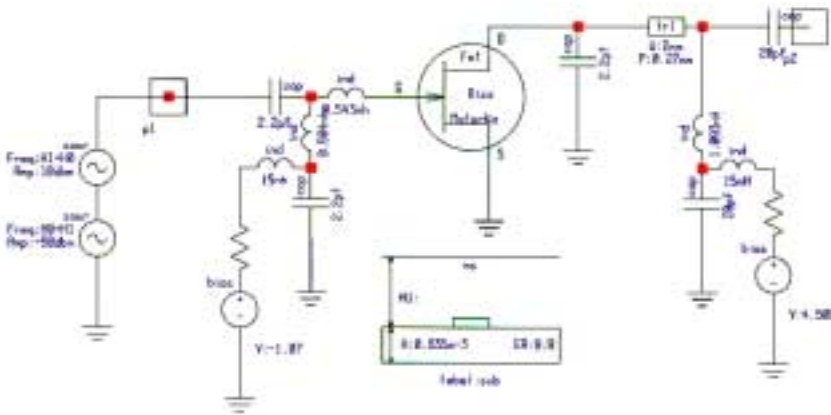


Figure 33--Nonlinear noise analysis of a mixer with a similar topology.

The length of the transmission line for a $\lambda/4$ resonator depends also on its reactive loading--specifically, the variations occurring during the manufacturing process. Some designers allow themselves some leeway to compensate for this as illustrated by Figure 34, which shows a 39-GHz two-stage oscillator. The matching network between the two stages, as well as the variable resonator, can be seen.

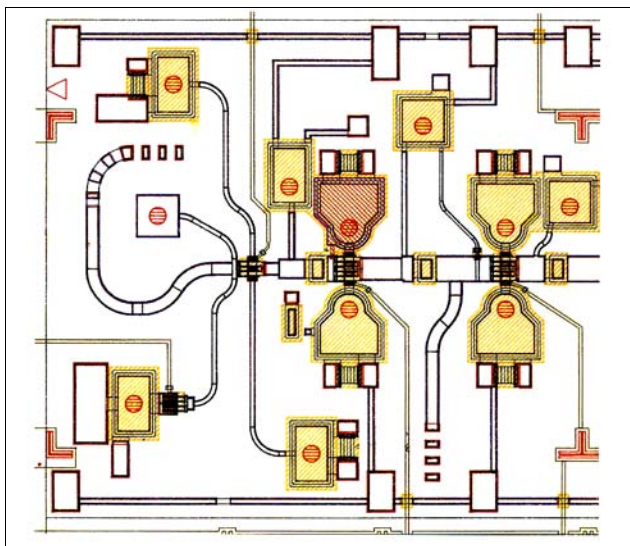


Figure 34--Layout of an experimental 39-GHz oscillator. The sequence of pads at the upper left allows production-line trimming of the actual length of the resonator.

The Microwave Clapp-Gouriet Oscillator

We have seen a variation of the Colpitts oscillator that, by adding a capacitor in series with the main inductance, is preferred in microwave applications. This oscillator type is called the Clapp-Gouriet, and most microwave engineers probably have never heard this name. Figure 35a shows the schematic of such an oscillator, which uses transmission lines for its resonator and several RF chokes. Figure 35b shows a simplified version.

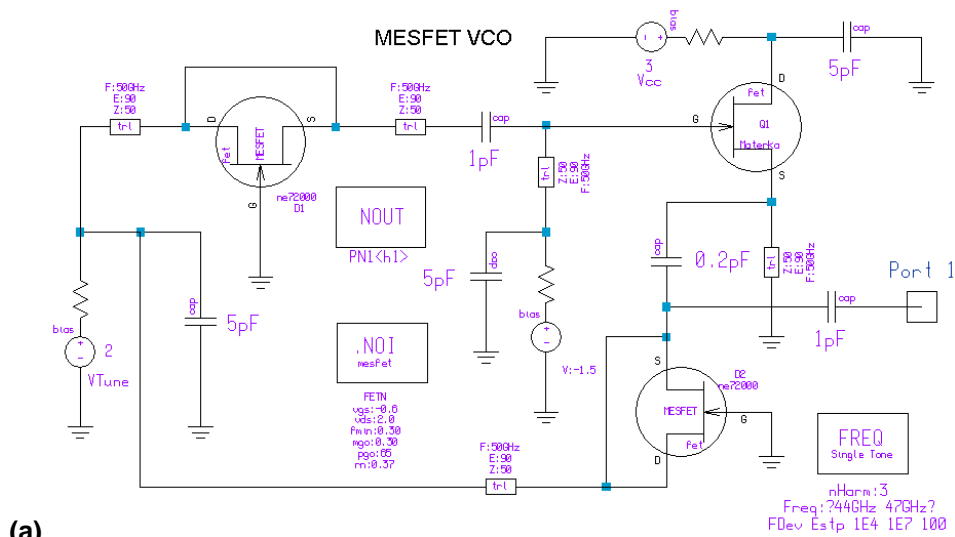
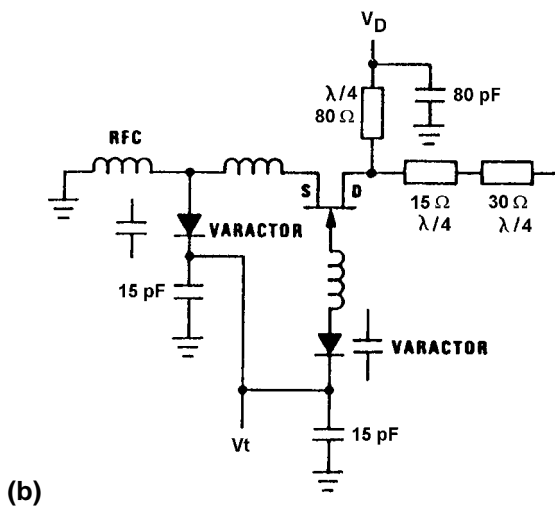


Figure 35(a)--Schematic of the 47-GHz MESFET oscillator using transistors instead of varactor (tuning) diodes--a nontrivial case for the harmonic-balance simulator.



35(b)—A simplified version, in which the output power is obtained from the collector.

The varactors are actually obtained by using the paralleled source-gate and drain-gate capacitances of additional GaAsFETs. This type of varactor, as well as the pure GaAs varactor, is always noisy. Typical examples of GaAs varactors are shown in Figures 36 and 37.

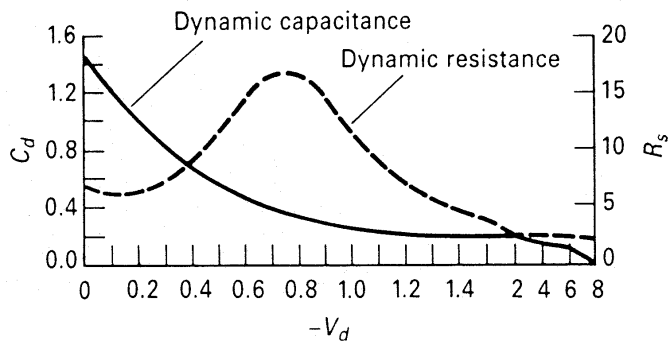


Figure 36--Dynamic capacitance and dynamic resistance as a function of tuning voltage for a GaAs varactor.

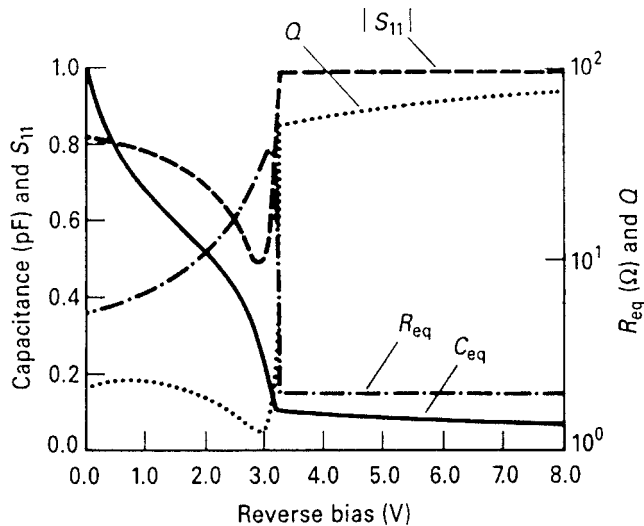


Figure 37--Varactor parameters: capacitance, equivalent resistance, and Q , as well as the magnitude of S_{11} as a function of reverse voltage.

It must be remembered that the noise contribution of such a "tuning diode" highly depends on its equivalent noise resistance--a value that cannot be measured with an ohmmeter. For microwave oscillators, the best way to determine this is to first build the oscillator without the varactor attached, measure its phase noise, and then measure the phase noise with the "diode" connected. The resulting deterioration is the contribution of the tuning diode.

An early example of the dual-varactor type oscillator is shown in Figure 38. The transistor is at the upper left; the resonator inductance goes to one "varactor," and the second "varactor" is above the transistor. This oscillator operated at 20 GHz and was designed by Texas Instruments.

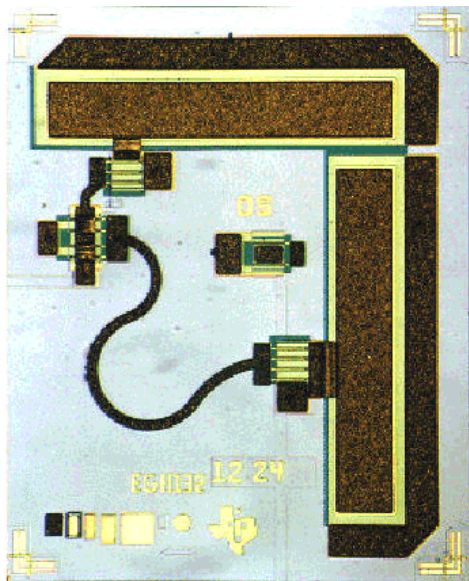


Figure 38--MESFET-based oscillator. The S-shaped transmission line acts as the resonator, and the circuit uses two tuning diodes for wider tuning range. Both GaAs varactors, as well as GaAsFETs used as varactors, have a high contribution to the resulting phase noise and limit the performance of the circuit.

Analyzing our Clapp-Gouriet microstrip-based oscillator, which we have optimized for 47 GHz, we obtain the phase noise as shown in Figure 39. (This is an oscillator circuit; to change it into a VCO, tuning diodes, which will make it noisier, must be added.) The curve has the familiar breakpoint, which is caused by the flicker noise of the transistor. It is a misconception to assume that the flicker corner frequency and the breakpoint will coincide. Because of the resonator Q , the breakpoint always occurs closer to the carrier. Only for very low Q s will the two values be the same.

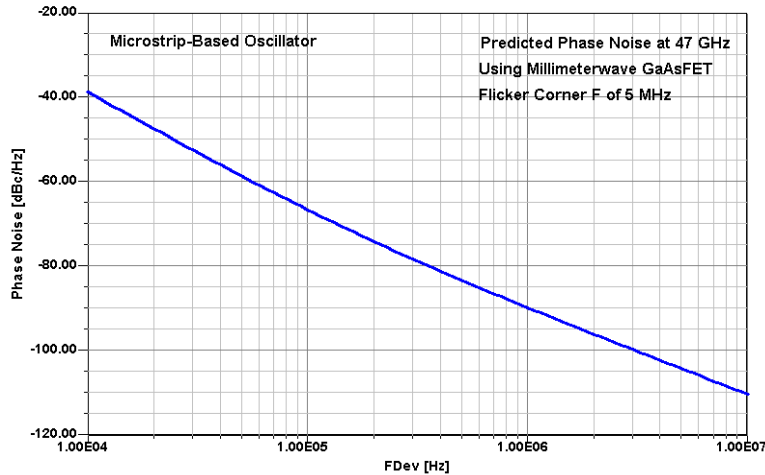


Figure 39--Assuming a flicker corner frequency of 5 MHz (optimistic), we can predict this phase noise response. The flicker frequency is responsible for the bend in the curve.

In the same fashion, we have used Ansoft Serenade's Oscillator Design Aid to predict the oscillation frequency. The resulting curves (Figure 40) are quite startling because of the discontinuities in the real and imaginary portions of the test current. They indicate the severe nonlinearities introduced by the GaAsFET oscillator transistor and the two "tuning diodes." Also, this time the peaks in the test current components are below the oscillation point; this is contrary to Figure 19, where the "resonance" occurs above this point. It clearly indicates that the oscillator has not been optimized for best operating Q --a task we gladly leave to the reader as a good challenge.

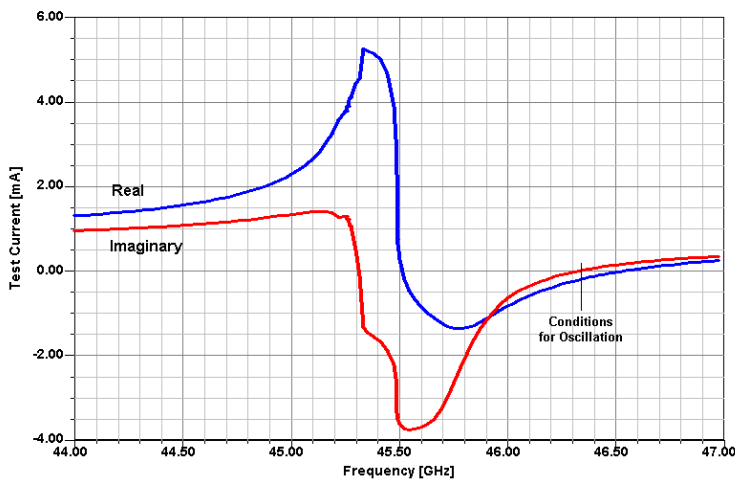


Figure 40--Test currents for finding the oscillating conditions of the 47-GHz oscillator. The actual linear prediction is 46.3 GHz; the large-signal condition then shifts the result towards 47 GHz. The strange curves are due to the highly nonlinear operation, including the two transistors acting as tuning diodes.

The next logical step is to look at the output spectrum (Figure 41). The attenuation of the second harmonic is the familiar 20 dB. The output was taken from the resonator circuit via the familiar capacitive divider. The drawback of this implementation will vary as a function of the capacitance of the varactor. A smarter, though somewhat complicated, way would be to magnetically couple from the resonator. This way, one obtains the best phase noise and has control over the loading. It is unclear why this method is not used for MMICs, while it is popular in circuits built with lumped elements and transmission-line resonators.

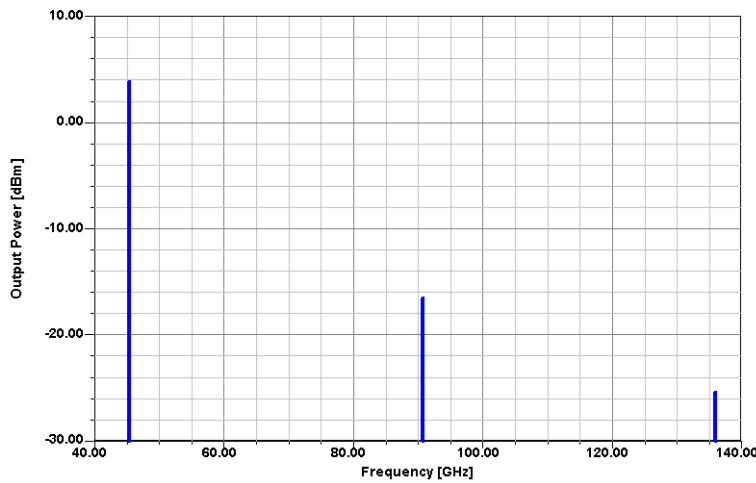


Figure 41--Predicted output spectrum for the 47-GHz FET-based oscillator.

The resulting phase noise, as anticipated, is poor and is characterized by a straight-line response (Figure 42). This is due to the diode noise contribution [the last term in (6)]. The phase noise of the oscillator is by far not state-of-the-art because the flicker noise and the diode noise are excessive. Current research in oscillators using SiGe transistors or even GaAs HBTs will result in much better phase noise performance.

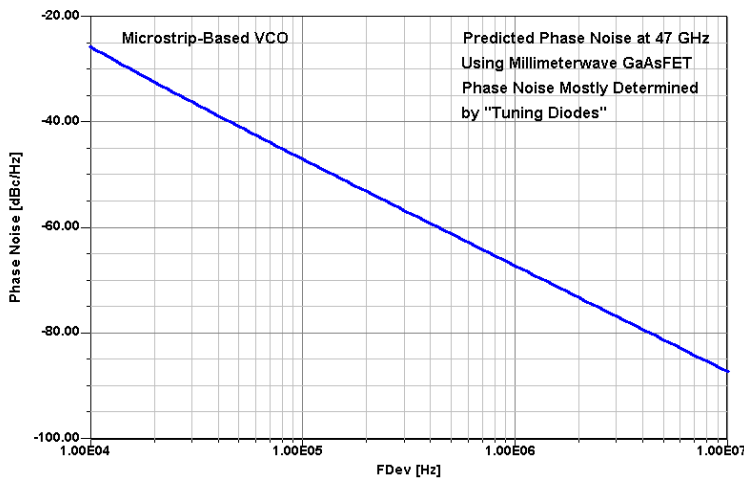


Figure 42--Predicted phase noise of the 47-GHz millimeterwave oscillator using GaAsFETs as tuning diodes. They are notoriously noisy.

Compared to Figure 39, we have lost our good phase noise performance.

Finally, we let the circuit simulator provide us with the oscillator transistor load line (Figure 43). By inspecting it, we see that the resulting ellipse is not limited either by current or voltage, which leads to low-distortion operation for the transistor. On the other hand, our previous examination showed strong nonlinearities. The reason why the ellipse is not distorted has to be the loose coupling, and yet the Q is low because of the resonator elements--specifically, the transistors used as varactor diodes. These diodes have their own load lines, since both dc and ac voltages are fed to them. Figure 44 shows the resulting load lines. The reason for the difference in their diameters has to do with the fact that power levels at the two points are different.

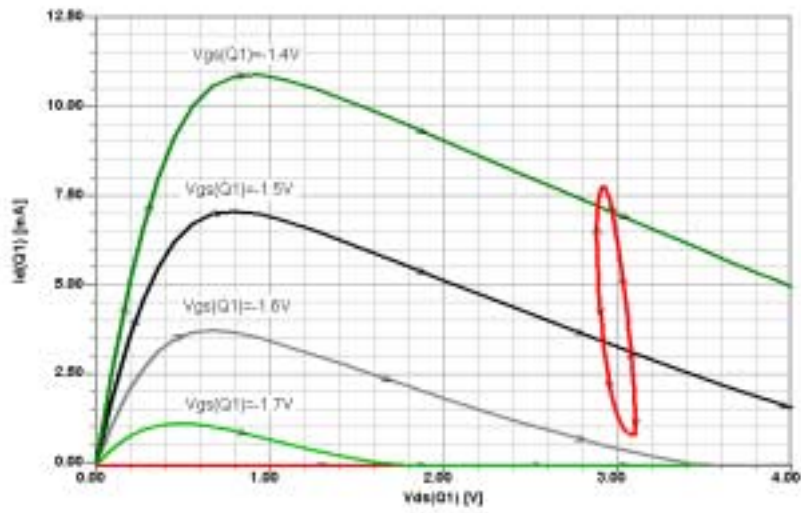


Figure 43--Dc I - V curves and load line for the oscillating FET in the 47-GHz VCO.

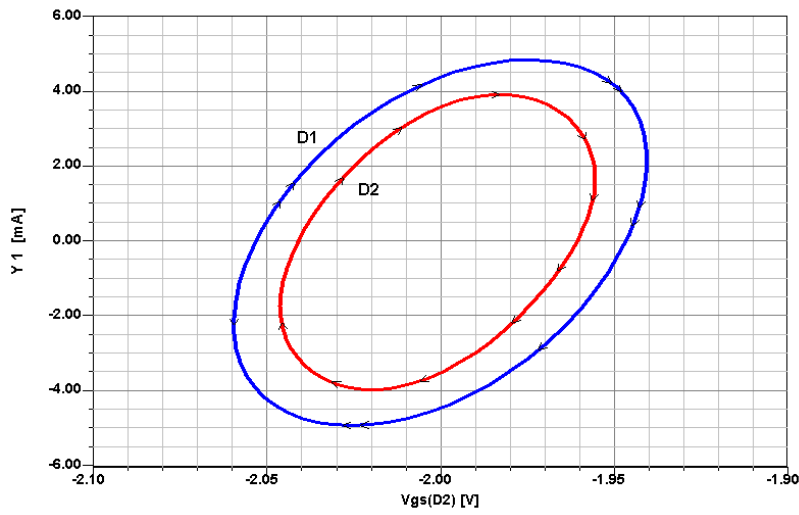


Figure 44--Load lines for the "tuning diodes" D1 and D2, which in reality are GaAsFETs with source and drain tied together. The round shape indicates that the "varactors" are both operating in their linear regions, but the devices themselves are highly nonlinear.

The circuit we just looked at, for simulation purposes, uses actual tuning diodes and transmission lines as resonators is shown in Figure 45.

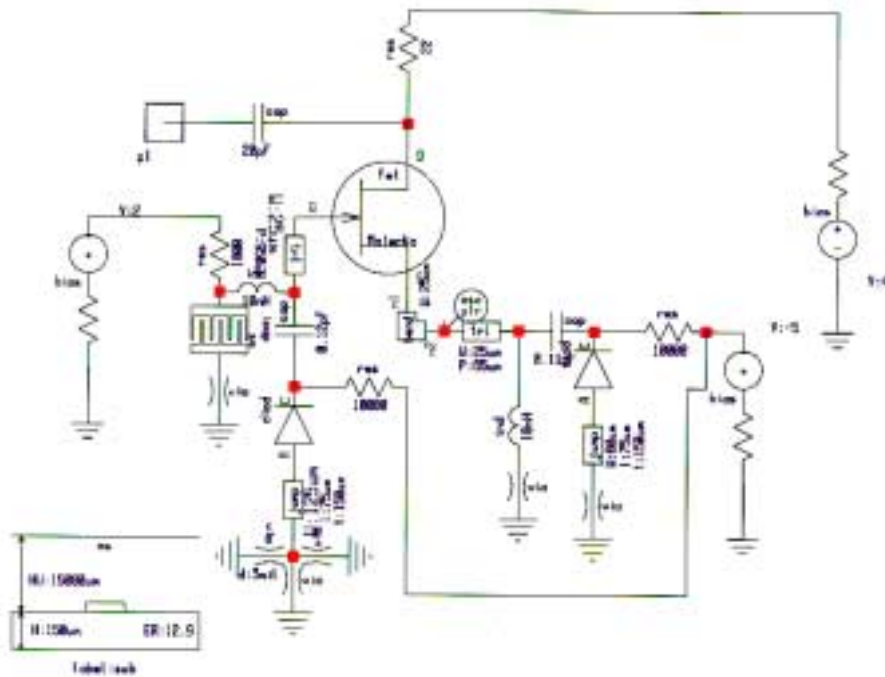


Figure 45--Detailed modeling of the two-diode TI VCO.

Conclusion

Designing microwave and millimeterwave oscillators still involves the use of some black magic, but a good understanding of their theory of operation, including a good simulator, does help. We have covered both bipolar transistors and GaAsFETs and point out their unique behavior. The oscillators we have used to demonstrate the design process were single-stage types. During the early mentioned MIMIC project, a variety of interesting oscillators was developed by members of the consortium. A very "colorful" one is shown in Figure 46. It is a ring type of oscillator using two transistors on each side and a combining circuit. The measured data agrees quite well with the simulation. Because this Ka-band MMIC VCO for smart munitions applications falls under export restrictions, only sketchy information can be provided. It employs a 0.25- μm gate length PHEMT.

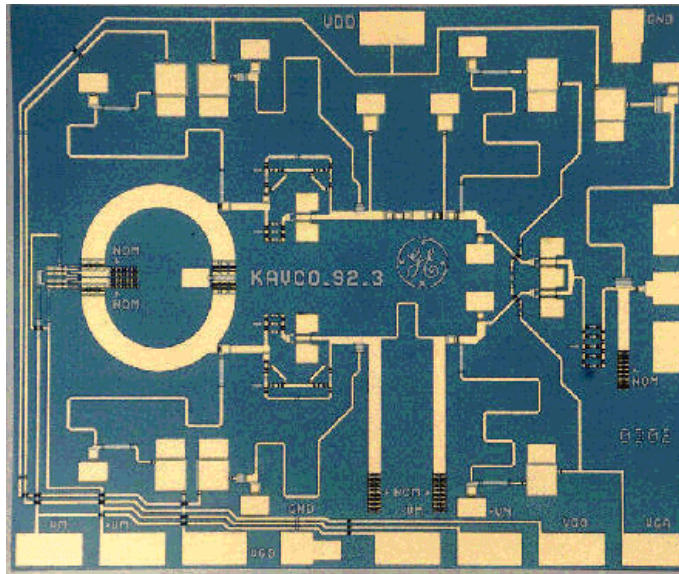


Figure 46-Fundamental-mode, differential ring VCO developed by Martin Marietta under the US Government MIMIC program. The CAD solutions were provided by Compact Software (now Ansoft). The oscillator features include: frequency range, Ka band; output power, 16 dBm minimum; electronically tunable; output power > 16 dBm; 13% power-added efficiency (PAE); compact size for easy integration with power amplifier; 0.25- μm pseudomorphic HEMTs.

In the area of SiGe transistors, the oscillator developed by Dr. Rheinfelder of DASA has already been mentioned. Using the properties of gallium arsenide as an MMIC material, one can predict the phase noise. If built all in silicon, the $1/f$ noise of the resistive area would make the noise even worse. Our last figure (Figure 47) shows the predicted phase noise of the Rheinfelder oscillator with a resonator Q of 7 (because of loading by the tuning diodes) and established with the ring oscillator of Figure 34 (a VCO), an assumed Q of 25. Finally, the plot also shows the measured data point at 100 kHz to be -93 dBc/Hz. At first glance, this measured data point does not seem to be real; however, it shows the power of modern simulation even at these frequencies. Also, it validates a Q of 70, which the author did not mention in his paper. Probably the best design procedure for microwave oscillators in the X band is shown in [15,16,17], which shows the best published results for a free-running microwave oscillator at room temperature with a pHEMT transistor.

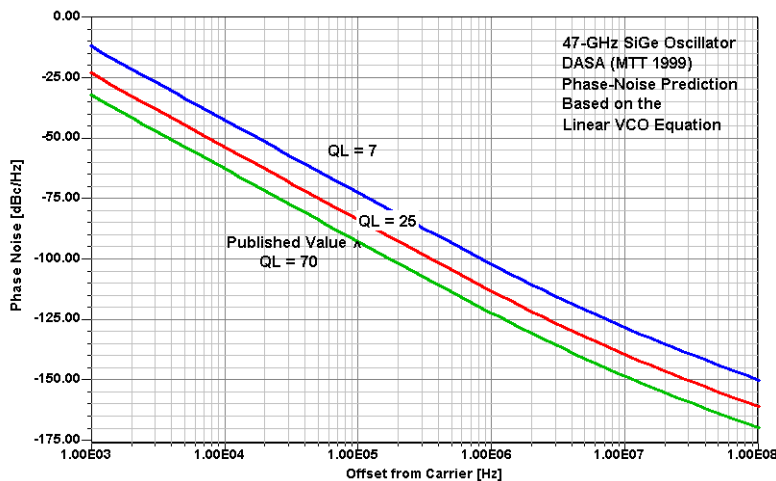


Figure 47--Predicted phase noise for Q_L s of 7 and 25 of the 47-GHz SiGe oscillator by Rheinfelder and others compared to the published and measured results ($Q_L = 70$, spot measurement indicated by the arrow).

References

1. Aron Kain, *Final Report for Bias Dependence Noise Modeling of Heterojunction Bipolar Transistors*, USAF SBIR Phase II (PIIN), F33615-95-C-1707, November 1997. Issued by USAF/AFMC/ASC, Wright Laboratory WL/AAKE BLD 7, 2530 C ST, Wright-Patterson AFB, OH 45433-7607.
2. Robert A. Pucel and Ulrich L. Rohde, "An Accurate Expression for the Noise Resistance R_n of a Bipolar Transistor for Use with the Hawkins Noise Model," *IEEE Microwave and Guided Wave Letters*, Vol. 3, No. 2, February 1993, pp. 35-37.
3. Robert A. Pucel, W. Struble, Robert Hallgren and Ulrich L. Rohde, "A General Noise De-embedding Procedure for Packaged Two-Port Linear Active Devices," *IEEE Transactions on Microwave Theory and Techniques*, Vol. 40, No. 11, November 1993, pp. 2013-2024.
4. C. N. Rheinfelder et alia, "47-GHz SiGe MMIC Oscillator," *1999 IEEE MTT-S Digest*, pp. 5-8.
5. V. Rizzoli, F. Mastri, and C. Cecchefti, "Computer-Aided Noise Analysis of MESFET and HEMT Mixers," *IEEE Transactions on Microwave Theory and Techniques*, Vol. MTT-37, September 1989, pp. 1401-1410.
6. V. Rizzoli and A. Lippadni, "Computer-Aided Noise Analysis of Linear Multiport Networks of Arbitrary Topology," *IEEE Transactions on Microwave Theory and Techniques*, Vol. MTT-33, December 1985, pp. 1507-1512.
7. V. Rizzoli, F. Mastri, and D. Masotti, "General-Purpose Noise Analysis of Forced Nonlinear Microwave Circuits," published in *Military Microwave*, 1992.
8. Ulrich L. Rohde, "Improved Noise Modeling of GaAs FETs," *Microwave Journal*, November 1991, pp. 87-101 (Part I) and December 1991, pp. 87-95 (Part II).
9. Ulrich L. Rohde, Chao-Ren Chang, and Jason Gerber, "Design and Optimization of Low-Noise Oscillators Using Nonlinear CAD Tools," *1994 IEEE International Frequency Control Symposium*, pp. 548-554.
10. Ulrich L. Rohde, "Oscillator Design for Lowest Phase Noise," *Microwave Engineering Europe*, May 1994, pp. 31-40.
11. Ulrich L. Rohde, *Microwave and Wireless Synthesizers: Theory and Design* (New York: John Wiley & Sons, 1997, ISBN 0-471-52019-5), Section 5-3 (Low-Noise Microwave Synthesizers) and Appendix B (A General-Purpose Nonlinear Approach to the Computation of Sideband Phase Noise in Free-Running Microwave and RF Oscillators).
12. Ulrich L. Rohde and David P. Newkirk, *RF/Microwave Circuit Design for Wireless Applications*, by John Wiley & Sons, April 2000, ISBN 0471298182.
13. F. X. Sinnesbichler et alia, "A 50-GHz SiGe HBT Push-Push Oscillator," *1999 IEEE MTT-S Digest*, pp. 9-12.

14. M. C. E. Yagoub and H. Baudrand, "Nonlinear Oscillator Design for Maximum Power," *1994 IEEE International Frequency Control Symposium*, pp. 555-558.
15. M. Prigent et alia, "An Efficient Design Method of Microwave Oscillator Circuits for Minimum Phase Noise," *IEEE Trans. Microwave Theory Tech.*, Vol. MTT-47, No. 7, July 1999, pp. 1123-1125.
16. M. Prigent and J. Obregon, "Phase Noise in FET Oscillators by low Frequency Loading and Feedback Circuitry Optimization," *IEEE Trans. Microwave Theory Tech.*, Vol. MTT-35, Mar. 1987, pp. 127-129.
17. E. Vaury et alia, "A New Method for the Design of Ultra Low Noise Oscillators," in *Int. Frequency Control Symp.*, Besançon, France, Apr. 1999.
18. Ulrich L. Rohde and Guenther Klage, "Analyze VCOs and Fractional-N Synthesizers," *Microwaves & RF*, August 2000, Pg. 57